# Guided-mode phonon-polaritons in suspended waveguides

Scott A. Holmstrom
*Department of Physics and Engineering Physics, University of Tulsa, Tulsa, Oklahoma 74104, USA*

Todd H. Stievater, Marcel W. Pruessner, Doewon Park, and William S. Rabinovich
*Naval Research Laboratory, Washington DC 20375, USA*

Jacob B. Khurgin
*Department of Electrical Engineering, Johns Hopkins University, Baltimore, Maryland 21218, USA*

Christopher J. K. Richardson, Subramaniam Kanakaraju, and Lynn C. Calhoun
*Laboratory for Physical Sciences, University of Maryland, College Park, Maryland 20740, USA*

Reza Ghodssi
*Department of Electrical and Computer Engineering, Institute for Systems Research, University of Maryland, College Park, Maryland 20742, USA*

(Received 14 November 2011; revised manuscript received 19 September 2012; published 15 October 2012)

We report on the characterization of two-dimensionally confined phonon-polaritons at terahertz frequencies in suspended waveguides using Raman scattering. The cross-sectional dimensions of the waveguides are commensurate with the wavelength of the phonon-polariton in forward scattering leading to Raman spectra that depend strongly on the physical size of the waveguide. We use finite element numerical computations to predict the polariton frequencies and find excellent agreement with measurements. Our observations and analysis advance the understanding of polariton propagation in guiding geometries and also have significant practical implications in integrated terahertz generation and stimulated Raman amplification.

DOI: 10.1103/PhysRevB.86.165120 PACS number(s): 42.82.Et, 71.36.+c, 63.22.−m, 78.30.−j

The phonon-polariton is a collective excitation comprised of an electromagnetic (EM) wave coupled with a polar lattice vibration. It can be understood in terms of an anticrossing of the constituents' dispersion curves in the material and, as such, is most pronounced when the optical and material vibrations have commensurate frequencies and wavelengths. For many materials of interest, this occurs at frequencies in the terahertz (THz) spectral range. Early observations of this type of polariton[1,2] in bulk crystals in the 1960s were closely followed by a number of studies focusing on polaritonic confinement and guiding in thin film geometries.[3–7] These latter studies distinguished confined polaritons from their bulk counterparts and reported on the existence of surface polaritons. Recently, there has been a resurgence in studies related to the phonon-polariton spurred by an increased interest in THz production[8–13] and imaging[14,15] in an integrated platform. Integrated polaritonics[16] has the potential to revolutionize next-generation devices operating in the THz portion of the electromagnetic spectrum in much the same way that integrated electronics and integrated photonics have revolutionized the microwave and near-infrared regimes, respectively. To date, though a number of research groups have demonstrated THz generation and propagation in waveguides, there has been no description of polaritonic dispersion, polarization, and modal confinement in fully guided, integrated geometries.

In this work, we show that the forward-scattering Raman spectra from indium phosphide (InP) waveguides contain clear evidence of scattering from guided-mode phonon-polaritons (GMPPs) at THz frequencies and elucidate their modal character through measurements on rectangular waveguides having a variety of cross-sectional dimensions. This characterization is made possible by the use of waveguides suspended in air (see Fig. 1) that tightly confine not only the near-infrared (NIR) pump and Stokes signal radiation but also the THz polaritonic radiation that couples the two NIR waves. The large index contrast of the suspended waveguides also serves to efficiently capture the Stokes-scattered signal radiation resulting in strong Raman spectra along the waveguide direction. In our analysis, we propose and experimentally verify a model for waveguide Raman scattering that is analogous to the plane wave method introduced by Henry and Hopfield[1] to predict the frequency of the bulk polariton.

Before we present our observations and analysis for the waveguide structures, it is instructive to discuss what would be expected for plane wave Raman scattering in bulk InP for our geometry and point out the very important difference between forward and backward scattering. Consider a plane wave traveling in the $[0\bar{1}1]$ ($\hat{z}'$) crystallographic direction with polarization along [100] ($\hat{x}$) or [011] ($\hat{y}'$) that undergoes scattering either directly forward or directly backward. These axes are the same as defined in Fig. 1. In this situation, there are four independent (incident, scattered) polarization combinations to consider: $(\hat{x},\hat{x})$, $(\hat{x},\hat{y}')$, $(\hat{y}',\hat{x})$, $(\hat{y}',\hat{y}')$. Bulk Raman selection rules[17] dictate that there should be scattering from a $y'$-polarized transverse optical (TO) vibration for the $(\hat{x},\hat{y}')$ and $(\hat{y}',\hat{x})$ combinations, scattering from an $x$-polarized TO vibration for the $(\hat{y}',\hat{y}')$ combination, and no Raman signal for $(\hat{x},\hat{x})$. Scattering by longitudinal optical (LO) phonons is forbidden by symmetry in the bulk for scattering along $\pm\hat{z}'$.

Wave vector conservation dictates that the TO material vibrations for the backward and forward scattered Raman have very different wavelengths, $\mathcal{O}(.1\,\mu\text{m})$ and $\mathcal{O}(10\,\mu\text{m})$,

 

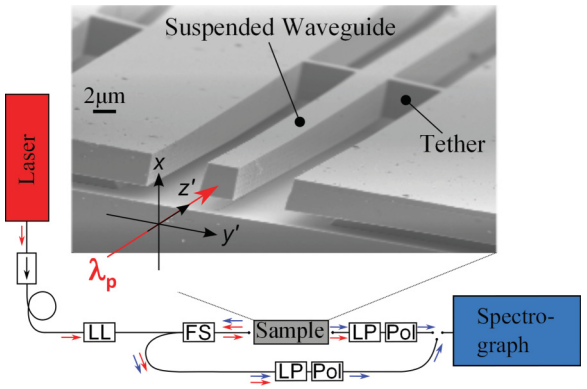


FIG. 1. (Color online) Scanning electron micrograph of a 2.5 × 4.0 $\mu$m (width × thickness) suspended waveguide, along with the coordinate system used for discussion and analysis. $z'$ corresponds to the [0$\bar{1}$1] crystallographic direction along the waveguide, $y'$ is the [011] direction, and $x$ is the [100] direction. In the experimental schematic, LL = laser-line filter, FS = fiber splitter, LP = long-pass filter, and Pol = linear polarizer. Forward-scattered or backward-scattered Raman spectra were measured, in separate experiments, by switching the fiber coupled to the spectrograph. The excitation laser provided 4 mW to the input facet of the waveguide and the spectrometer was equipped with a liquid-nitrogen-cooled InGaAs detector array.

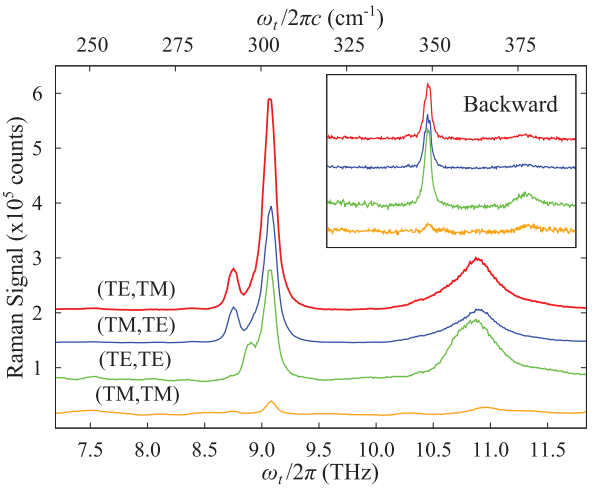


FIG. 2. (Color online) Raman spectra ($\lambda_p$ = 1054 nm) for forward scattering in a 5.3 × 2.5 $\mu$m waveguide. Each plot except (TM,TM) has been offset vertically for clarity in presentation. The small signal in (TM,TM) is an indication of polarization mixing in the experiments. The inset shows the backward-scattering spectra ($\lambda_p$ = 1460 nm) in the same waveguide.

respectively, for our material, and hence different coupling strengths with EM waves. For backward scattering, the wavelength is too small to couple strongly with EM waves so the Raman-scattered light would be shifted from the pump by the *pure* TO frequency in InP, $\omega_{TO} = 303$ cm$^{-1}$. For forward scattering, the wavelength is right in the heart of the anticrossing region so the Raman-scattered light would be shifted from the pump by the bulk phonon-polariton frequency at this wavelength; ~250 cm$^{-1}$ for our material. We will compare our observations in the waveguides with these predictions for the bulk.

The waveguides used in this work were fabricated by molecular beam epitaxy. A layer of $n$-doped[18] InP (either 2.5 $\mu$m or 4.0 $\mu$m thick) was grown on a 2-$\mu$m-thick layer of sacrificial InGaAs. By patterning and etching the InP and then selectively etching the InGaAs, the rectangular cross-section InP waveguides are suspended above the substrate supported by lateral tether pairs distributed along their length, as shown in Fig. 1. Details of the fabrication can be found in Ref. 19. More than fifty waveguides of this sort, with a variety of cross-sectional aspect ratios, have been studied for this work.

Tapered polarization-maintaining fibers were used to couple light into and out of the waveguides and were aligned to maximize throughput of the pump laser in the fundamental mode. Waveguide modes supporting polarization predominantly along the $x$ axis will be referred to as TM$_{mn}$ modes and those supporting polarization predominantly along the $y'$-axis as TE$_{mn}$ modes, where $m$ and $n$ are the number of field zeros in the $y'$ and $x$ directions, respectively. We used laser excitation of the TE$_{00}$ or TM$_{00}$ mode at the pump frequency and monitored the Raman signal scattered into TE or TM modes at the Stokes frequency. This scattering will be denoted by ($X$,$Y$) where $X$ and $Y$ represent the pump mode and the scattered mode polarizations, respectively.[20] The TE and TM polarization designations will also be used below to describe the GMPP modes.

Example forward-scattering, waveguide Raman spectra for all polarization combinations studied in this work are shown in Fig. 2. The corresponding backscattering spectra are shown in the figure inset over the same frequency range. We detect scattered light in the NIR but all the spectra are plotted versus Raman shift thereby indicating the frequency of the material vibration involved in the scattering. It is important to note that the backward-scattering spectra display a fraction of the forward-scattering signal, and vice versa, due to internal reflections at the waveguide facets. With this in mind, the backscattering spectra are consistent with bulk selection rules [i.e., they are dominated by single peaks at the TO phonon frequency (303 cm$^{-1}$)] for appropriate polarization combinations. The forward-scattering spectra, however, are significantly different than predicted for a bulk material.

Although not the the emphasis of this report, the broad feature above 10 THz in these spectra is noteworthy because it is significantly enhanced for forward scattering due to confinement effects. This peak is consistent with scattering with LO phonons and we assert that it arises due to mixing of TO and LO vibrations at the confining surfaces of the waveguide. Mixing of TO and LO phonons at material interfaces, which occurs when the TO polarization direction has a nonzero component along the normal to the interface, has been well documented.[21–24] In our material, which is lightly $n$-doped, the confinement-induced TO/LO mixing feature doesn't appear at the LO phonon frequency (345 cm$^{-1}$) as it would for an undoped material; it is shifted to higher energies (and broadened) through interactions with free carriers. This collective excitation is referred to as an LO phonon-plasmon coupled mode.[25] The LO phonon-plasmon feature is less evident in backscattering spectra because the TO wavelengths are two orders of magnitude smaller than for forward scattering. It is discernible, however, in (TE,TE) backscattering because the

material vibration in this case is polarized along $x$ and mixes with LO via the vertically confining surfaces that are only 2.5 $\mu$m apart. (TE,TM) and (TM,TE) scattering both produce material vibrations polarized along $y'$.

The focus of this report is the multipeaked features below 10 THz in Fig. 2, which we propose are consistent with scattering by GMPPs in a variety of waveguide modes. In particular, we associate the resolved peaks at 8.75 THz in (TE,TM) and (TM,TE) and at 8.90 THz in (TE,TE) with the production of a GMPP in its *fundamental* TE and TM waveguide mode, respectively. As we show below, this spectral feature can change significantly with changes in the cross-sectional dimensions of the waveguide.

We propose here that for waveguide Raman scattering in which pump light at frequency $\omega_p$ is converted into a THz signal at $\omega_t$ (the GMPP) and a light wave at the Stokes-shifted frequency $\omega_s = \omega_p - \omega_t$, the observed Raman resonances can be accurately predicted by the intersection of the GMPP dispersion and three-wave-mixing phase-matching curves for each set of modes. We now outline our guided-mode model for Raman scattering in the waveguides that accurately predicts the position of these peaks as a function of waveguide cross section.

Since the pump light, the collected scattered light, and the phonon-polariton are all guided in our experiment, we have to consider GMPP dispersion curves and phase-matching curves for all physically reasonable mode combinations. Using wave vector and energy conservation, the modal phase-matching (PM) equation for waveguide Raman Stokes scattering can be written as

$$k_{t:mn}^{(\mathrm{PM})}(\omega_t) = \frac{\omega_p}{c} n_{\mathrm{eff}:00}(\omega_p) - \frac{(\omega_p - \omega_t)}{c} n_{\mathrm{eff}:mn}(\omega_p - \omega_t), \tag{1}$$

where $k_{t:mn}^{(\mathrm{PM})}(\omega_t)$ is the magnitude of the effective GMPP wave vector in its $\mathrm{TE}_{mn}$ or $\mathrm{TM}_{mn}$ waveguide mode at $\omega_t$, $n_{\mathrm{eff}:ij}(\omega)$ is the effective index for the $\mathrm{TE}_{ij}$ or $\mathrm{TM}_{ij}$ mode evaluated at $\omega$, and $c$ is the speed of light in vacuum. A finite-element electromagnetic mode solver (COMSOL MULTIPHYSICS) was used to calculate the effective modal indices found in Eq. (1). In these calculations, the first-order Sellmeier equation for $n$-doped InP[26] was used as the dielectric function of the waveguide structures, extrapolated to the appropriate doping level for our material. To produce a phase-matching curve for a particular scattered mode, $n_{\mathrm{eff}:00}(\omega_p)$ was calculated along with $n_{\mathrm{eff}:mn}(\omega_p - \omega_t)$ over an appropriate range of Stokes-shifted frequencies yielding a table of the kinematically possible GMPP frequencies ($\omega_t/2\pi$) that could then be plotted versus $k_{t:mn}^{(\mathrm{PM})}$ using Eq. (1).

The GMPP dispersion curves near the THz difference frequency, $\omega_t$, were also calculated using the finite-element mode solver. In this case, the effective mode indices were calculated for a range of difference frequencies near 9 THz and were then used to construct the dispersion (D) curve according to

$$k_{t:mn}^{(D)}(\omega_t) = \frac{\omega_t}{c} n_{\mathrm{eff}:mn}(\omega_t). \tag{2}$$

The dielectric function used for these calculations accounts for optical phonon resonances and plasmonic effects from the free carriers[25,27] and is given by

$$\epsilon(\omega) = \epsilon_\infty \left(1 + \frac{\omega_{\mathrm{LO}}^2 - \omega_{\mathrm{TO}}^2}{\omega_{\mathrm{TO}}^2 - \omega^2 - i\omega\Gamma_t} - \frac{\omega_e^2}{\omega^2 + i\omega\Gamma_e}\right), \tag{3}$$

where $\epsilon_\infty$ is the high-frequency dielectric constant, $\omega_{\mathrm{TO}}$ and $\omega_{\mathrm{LO}}$ are the angular frequencies of the TO and LO lattice vibrations, $\Gamma_t$ and $\Gamma_e$ are the phonon and plasmon line widths, and $\omega_e$ is the Drude plasma frequency given by $\omega_e^2 = (N_c q^2)/(\epsilon_\infty m_{\mathrm{eff}} \epsilon_0)$, where $N_c$, $q$, and $m_{\mathrm{eff}}$ are the free carrier number density, charge, and effective mass, and $\epsilon_0$ is the permittivity of free space. The values for the parameters we used in Eq. (3) were $\epsilon_\infty = 9.61$,[28] $m_{\mathrm{eff}} = 0.074 m_e = 9.1 \times 10^{-34}$ kg,[28] $N_c = 5.0 \times 10^{23}$ m$^{-3}$ (nominal), and the experimentally measured values $\omega_{\mathrm{TO}} = 5.71 \times 10^{13}$ s$^{-1}$ (303 cm$^{-1}$), $\omega_{\mathrm{LO}} = 6.50 \times 10^{13}$ s$^{-1}$ (345 cm$^{-1}$), $\Gamma_p = 6.0 \times 10^{11}$ s$^{-1}$ (3.2 cm$^{-1}$), and $\Gamma_e = 2.6 \times 10^{12}$ s$^{-1}$ (14 cm$^{-1}$).

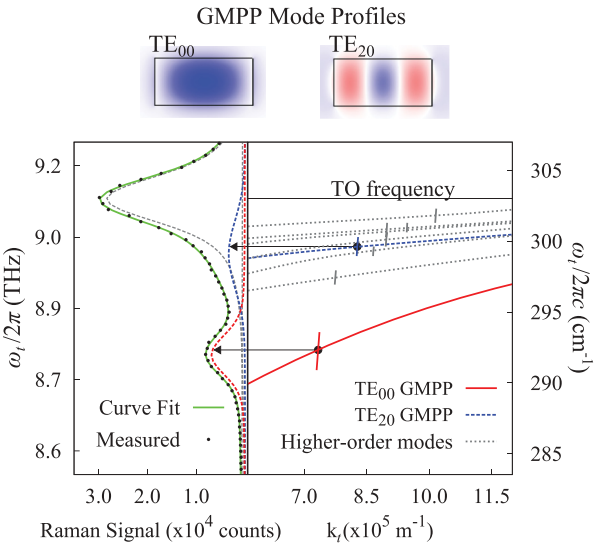


FIG. 3. (Color online) Top: Surface plots of $\mathrm{TE}_{00}$ and $\mathrm{TE}_{20}$ GMPP modes as calculated for a 5.3 × 2.5 $\mu$m waveguide at a frequency of 9.0 THz using COMSOL MULTIPHYSICS. Left panel of graph: Collected (TM,TE) Raman spectrum (dots) for a 5.3 × 2.5 $\mu$m waveguide with curve fit (solid line) and the three constituent Lorentzian peaks of the fit (dashed lines). Right panel of graph: GMPP dispersion curves for several modes. Each dispersion curve is crossed by a nearly vertical line segment of the phase-matching curve according to Eq. (1) for a pump in the $\mathrm{TM}_{00}$ mode and the Stokes signal in the $\mathrm{TE}_{mn}$ mode.

Surface plots of calculated cross-sectional mode profiles for the two lowest-order even TE GMPP modes of a 5.3 $\mu$m × 2.5 $\mu$m waveguide are shown at the top of Fig. 3. The calculated GMPP dispersion curves for these modes and several higher-order modes are plotted in the right panel of Fig. 3. Crystal symmetry and modal overlap considerations[29] are consistent with the $\mathrm{TE}_{mn}$ Stokes signal scattered predominantly by the $\mathrm{TE}_{mn}$ GMPP. Accordingly, a section of the $\mathrm{TM}_{00}$ pump → $\mathrm{TE}_{mn}$ Stokes phase-matching curve is plotted on top of each $\mathrm{TE}_{mn}$ GMPP dispersion curve. The frequency of the crossing point of these two curves for each mode is the predicted polariton frequency for that mode.

The left panel of Fig. 3 shows experimental (TM,TE) Raman spectrum data points and our curve fitting results, including constituent Lorentzians, for comparison with calculation. As can be seen by comparing the left and right panels in the figure, the lowest frequency peak is identified with the $TE_{00}$ GMPP (solid red curve) while the broad shoulder feature just below 9.0 THz is consistent with an agglomeration of various higher-order GMPP modes as shown. The $TE_{20}$ GMPP (dashed blue curve) is thought to be the primary contributor to the observed Raman peak. We make this assignment because, as asserted above, the NIR signal for this scattering event would also be in a $TE_{20}$ mode and the signal collection fibers are aligned to maximize coupling with *even* waveguide modes. The largest spectral feature near the bulk TO frequency at 9.1 THz is due to the combined effects of forward scattering into all the higher-order GMPP waveguide modes (not shown) and backscattering signal reflected into the forward direction at the input waveguide facet.

As mentioned earlier, more than fifty waveguides of this sort, with a variety of cross-sectional aspect ratios, have been studied in this work. Figure 4 shows the measured $TE_{00}$ and $TM_{00}$ GMPP frequencies versus waveguide widths for the two different waveguide thicknesses studied in this work.

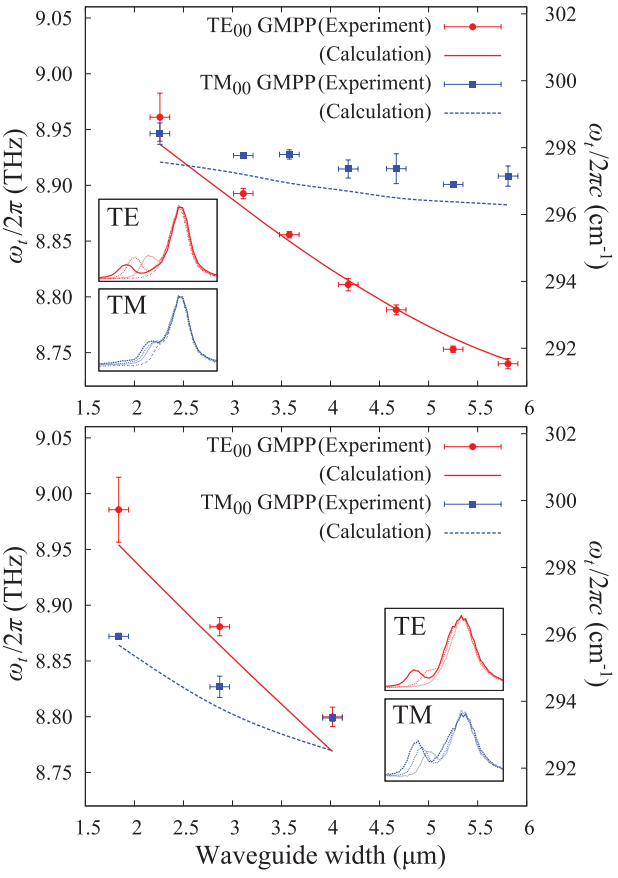


FIG. 4. (Color online) Upper panel: $TE_{00}$ and $TM_{00}$ GMPP frequency versus waveguide width for the 2.5-$\mu$m-thick waveguides. The insets show the normalized Raman spectra for a series of waveguide widths. Lower panel: $TE_{00}$ and $TM_{00}$ GMPP frequency versus waveguide width for the 4.0-$\mu$m-thick waveguides. The insets show the normalized Raman spectra for a series of waveguide widths.

The frequency values were obtained through peak fitting and the vertical error bars on the data points represent the distribution of measured GMPP frequency for waveguides with a nominal common width. The horizontal error bars represent the average variation of the waveguide's measured width along its length. For each physical waveguide width and thickness, a numerical calculation was performed to determine the expected GMPP frequency using only measured and/or accepted values for the parameters as detailed above. The solid red and dashed blue lines in Fig. 4 represent the results of these calculations.

In our experiments, we have studied ten different widths and two different thicknesses of waveguides but it is clear from our analysis that the generated THz frequency could generally be tuned using any method that alters the effective mode indices at the pump, Stokes, and/or THz frequencies. It is noteworthy from our data that the generated THz frequency is most strongly affected by changes in the material dimension along the GMPP polarization direction, with TE GMPPs affected strongly by width and TM GMPPs by thickness. This strong dependence is mimicked in the THz effective mode index calculation with $n_{\mathrm{eff}:mn}$ being very sensitive to changes in width for TE modes and thickness for TM modes. Confining surfaces along the direction of polarization are also responsible for the LO/TO phonon mixing mentioned earlier. The connection between these two phenomena is evidenced by comparing the top three Raman spectra shown in Fig. 2. The (TE,TM) and (TM,TE) scattering configurations result in nearly identical spectra because both produce a GMPP polarized along the 5.3-$\mu$m width. The (TE,TE) configuration, however, produces a GMPP polarized along the 2.5-$\mu$m thickness and, hence, shows significant differences not only in the GMPP fundamental mode but also in the LO phonon-plasmon mode. For a symmetric waveguide, these three spectra would be indistinguishable.

The results presented here not only advance the understanding of polaritons in guiding geometries but also have significant practical implications. A variety of three-wave-mixing approaches in semiconductor waveguides are under investigation for integrated THz sources[9,11,13,30] or stimulated Raman amplifiers.[31,32] In either case, efficient photon generation only occurs at difference frequencies corresponding to the intersection between the THz phase-matching curve and dispersion curve. Our results and analysis show how the properties of the waveguide itself are critically related to the allowed THz frequencies through the modal properties of the guided-mode polariton. For example, a difference-frequency-generation-based THz source at frequencies below the TO resonance can be implemented by coupling two laser sources with angular frequencies $\omega_p$ and $\omega_s$. A slotted, suspended waveguide can be employed to enable *in situ* MEMS tunability in the waveguide index and dispersion, which would in turn enable tunability in the frequency of phase-matched Thz generation.[33] Such stimulated polariton scattering is simply near-resonant difference-frequency generation using the ionic rather than electronic part of the second-order susceptibility $\chi_i^{(2)}(\omega_p,\omega_s;\omega_p-\omega_s)$ with the polariton generated at $\omega_p-\omega_s$ near $\omega_{\mathrm{TO}}$. The difference-frequency-generation efficiency would be limited by absorption, but significant THz generation could still be realized by continuously coupling the THz wave

out of the waveguide over length scales roughly equal to the absorption length, or simply by working at frequencies red enough from $\omega_{TO}$ to minimize loss. Furthermore, if a resonant cavity at the Stokes frequency comprised of distributed feedback mirrors along the length of the waveguide were employed, it should be possible to achieve optical parametric oscillation with only one CW laser input leading eventually to integrated, compact tunable THz sources.

This work was supported, in part, by the US Office of Naval Research.

[1]C. H. Henry and J. J. Hopfield, Phys. Rev. Lett. **15**, 964 (1965).
[2]W. L. Faust and C. H. Henry, Phys. Rev. Lett. **17**, 1265 (1966).
[3]K. L. Kliewer and R. Fuchs, Phys. Rev. **144**, 495 (1966).
[4]D. L. Mills, Y. J. Chen, and E. Burstein, Phys. Rev. B **13**, 4419 (1976).
[5]K. R. Subbaswamy and D. L. Mills, Solid State Commun. **27**, 1085 (1978).
[6]J. B. Valdez, G. Mattei, and S. Ushioda, Solid State Commun. **27**, 1089 (1978).
[7]Y. Sasaki and S. Ushioda, Phys. Rev. B **27**, 1122 (1983).
[8]T. Tanabe, K. Suto, Jun-ichi Nishizawa, K. Saito, and T. Kimura, Appl. Phys. Lett. **83**, 237 (2003).
[9]W. Shi and Y. J. Ding, Opt. Lett. **30**, 1030 (2005).
[10]K. Saito, T. Tanabe, Y. Oyama, K. Suto, and Jun-ichi Nishizawa, J. Appl. Phys. **105**, 063102 (2009).
[11]Jun-ichi Nishizawa, K. Suto, T. Tanabe, K. Saito, T. Kimura, and Y. Oyama, IEEE Photonics Technol. Lett. **19**, 143 (2007).
[12]J. Hebling, K.-L. Yeh, K. A. Nelson, and M. C. Hoffmann, IEEE J. Sel. Top. Quantum Electron. **14**, 345 (2008).
[13]G. Chang, C. J. Divin, J. Yang, M. A. Musheinish, S. L. Williamson, A. Galvanauskas, and T. B. Norris, Opt. Express **15**, 16308 (2007).
[14]N. S. Stoyanov, D. W. Ward, T. Feurer, and K. A. Nelson, Nature Mater. **1**, 95 (2002).
[15]T. Feurer, J. C. Vaughan, and K. A. Nelson, Science **299**, 374 (2003).
[16]T. Feurer, N. S. Stoyanov, D. W. Ward, J. C. Vaughan, E. R. Statz, and K. A. Nelson, Annu. Rev. Mater. Res. **37**, 317 (2007).
[17]R. Loudon, Adv. Phys. **50**, 813 (2001).
[18]The *n*-doping has no bearing on the ability to observe scattering by polaritons but does affect the relative positions of the observed Raman resonances.
[19]D. P. Kelly, M. W. Pruessner, K. Amarnath, M. Datta, S. Kanakaraju, L. C. Calhoun, and R. Ghodssi, IEEE Photonics Technol. Lett. **16**, 1298 (2004).
[20]In traditional plane wave Raman scattering nomenclature, the bracketed pump and scattered polarization directions would be flanked by pump and scattered propagation direction. In the waveguide geometry, where we observe only along the waveguide direction, these added designations are unnecessary.
[21]D. W. Berreman, Phys. Rev. **130**, 2193 (1963).
[22]J. E. Zucker, A. Pinczuk, D. S. Chemla, A. Gossard, and W. Wiegmann, Phys. Rev. Lett. **53**, 1280 (1984).
[23]A. Fainstein, P. Etchegoin, M. P. Chamberlain, M. Cardona, K. Tötemeyer, and K. Eberl, Phys. Rev. B **51**, 14448 (1995).
[24]T. Saito, K. Suto, Jun-ichi Nishizawa, and M. Kawasaki, J. Appl. Phys. **90**, 1831 (2001).
[25]L. Artús, R. Cuscó, J. Ibáñez, N. Blanco, and G. González-Díaz, Phys. Rev. B **60**, 5456 (1999).
[26]J. Stone and M. S. Whalen, Appl. Phys. Lett. **41**, 1140 (1982).
[27]P. Y. Yu and M. Cardona, *Fundamentals of Semiconductors: Physics and Material Properties*, 3rd ed. (Springer, Berlin, 2005).
[28]N. M. Schmidt, *Handbook Series on Semiconductor Parameters*, Vol. 1 (World Scientific, Singapore, 1996).
[29]B. Crosignani, P. DiPorto, and S. Solimeno, Phys. Rev. A **21**, 594 (1980).
[30]K.-H. Lin, C. A. Werley, and K. A. Nelson, Appl. Phys. Lett. **95**, 103304 (2009).
[31]K. Suto, T. Saito, T. Kimura, Jun-ichi Nishizawa, and T. Tanabe, J. Lightwave Technol. **20**, 705 (2002).
[32]R. Espinola, J. Dadap, J. Richard Osgood, S. McNab, and Y. Vlasov, Opt. Express **12**, 3713 (2004).
[33]J. B. Khurgin, M. W. Pruessner, T. H. Stievater, and W. S. Rabinovich, Opt. Lett. **33**, 2904 (2008).